The determination of the nanostructurated materials' morphology, by applying the statistics of the structural element maps

P. ZAMORA IORDACHE[a*], R. M. LUNGU[a], G. EPURE[a], M. MUREŞAN[a], R. PETRE[a], N. PETREA[a], A. PRETORIAN[a], B. DIONEZIE[b], L. MUTIHAC[c], V. ORDEANU[d]
[a]*Scientifical Research Centre for CBRN Defence and Ecology, 225, Olteniţei, Bucharest,Romania*
[b]*Politehnica University of Bucharest – Biomaterials Research Center, 313, Spl. Independentei, Bucharest,Romania*
[c]*University of Bucharest, Department of Analytical Chemistry, 4-12, Regina Elisabeta Blvd., 030018 Bucharest,Romania*
[d]*Medico-Military Scientifical Research Center, 37, C.A. Rosetti, Bucharest,Romania*

The obtaining of intelligent materials requires strict control of physical and chemical parameters that characterize them. In most cases, especially in the case of the nano- or microcomposite structures, the parameters to be controlled and quantified are of morphological and topological nature. This is a direct consequence of the fact that the chemical and physical properties of the nanoparticles and composite materials are strongly dependent on the geometric dimensions. In order to obtain certain material structures a strict control and conditioning of the nanostructured morphology and topology elements entering the composition of the material base is required. By controlling these parameters one may change the surface physical and chemical properties of the component structural elements (electrical and magnetical polarizability, interface free energy, etc.) so as to set a series of phase equilibria that should favour the obtaining of the desired structural properties. This paper proposes an analytical model for solving the morphology and topology which characterises the functionalized nanostructures. This model allows the establishment of analytical connections between real morphological and topological parameters, and the optoelectronically acquired data. Also, the analytic model allows the finding of its own values which characterize the morphological and topological structure of the nanostructure elements.

(Received May 10, 2011; accepted May 25, 2011)

Keywords: Nanoparticle morphology, Bulk domains, Flocculation, Chemical maps, Functionalisation procces

1. Introduction

Broadly speaking, the morphology can be defined as the science of shapes, whereas the topology is the science of their connectivity and variety. [4]. The mathematical morphology was founded by G. Matheron and J. Serra in 1964. Between the mathematical morphology and computational geometry there are a series of differences, which are generated by the fact that the concept of ''mathematical point", which in computational geometry is ascribed to finite dimensional entities. The determination and pattern recognition algorithms depend on the applied registration methods and techniques.

The correspondence between real objects and their real image f(x) is performed by means of a ψ operator, which is translation invariant (TI), and which is defined on a E (R^d, Z^d) domain.

Thus, for any f input signal and for each (h,v) set, belonging to ExR, one can define the relations [1]:

$$\psi(f_{h,v})= [\psi(f)]_{h,v},\ f_{h,v}(x):=f(x-h)+v \qquad (1)$$

The TI operator can be assigned the addition ($\delta;\oplus$) or extractions (ε; Θ) functions, so that the structural element g(x) can be defined, by means of the relations [1]:

$$\delta(f)=f\oplus g,\ \varepsilon(f)=f\Theta g \qquad (2)$$

$$(f\oplus g)(x)=\max\{g(x-z)+f(z) : z\in D[f]\} \qquad (3)$$

$$(f\Theta g)(x)=\min\{ f(z)-g_x(z)+: z\in D[g_x]\} \qquad (4)$$

All the fundamental morphological operations (e.g..: Hit-Miss, Open, Close, Boundary, Convex Hull, Skeleton, Thin, Thick, Prune) are defined by means of the operations $\oplus$ and Θ [13].

Fig. 1. Signal erosion by a nonflat structuring element[2]

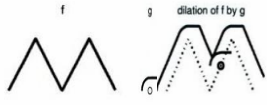

Fig. 2. Signal dilation by a nonflat structuring element[2].

The structural function is a derived concept of the notion of „adaptive morphology of the Euclidian space",

being applied to graphical, statistical, morphological and topological processing, of the "structural elements maps" type [1,5]. An A structural function assigns an *A(x)* set of functions to each x point from the space. The passage from a point in space to another can be modelled by one of the operators [2]: *adaptive window, adaptive kernel or adaptive weight* [2]. These types of operators are used during data computerized processing (images, etc.), involving space, energy, etc., adaptive operations as well as adjusting operatios of the analized domains [14]. The space-adaptive image processing operators, vary at the level of the entire image, with adaptive window scanning, according to the local structural features of the structural element maps. For example adaptive window scanning uses planar operators with spatial distributions of the A:E→P(E) type, and the operators of the *adaptive kernel and adaptive weight* use functions with fixed support, respectively different spatial distributions for the quantification of the structural elements of the elemental maps [1].

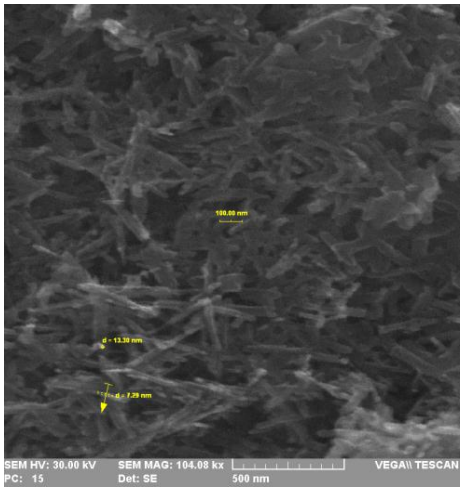

(a)

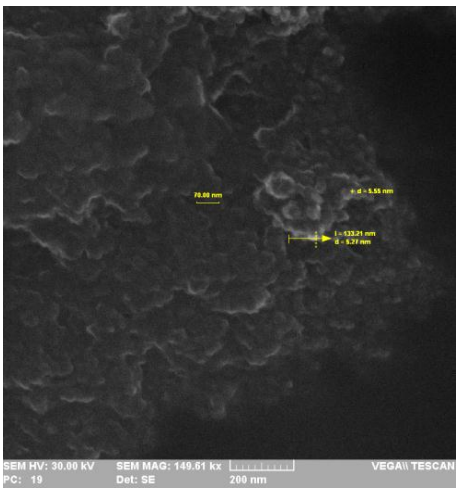

(b)

Fig. 3. Scanning electron image of the(ECH)$_{n\beta}$-npa-(GL)$_{n\varepsilon}$|$_{(Fe3O4\rightarrow CP)}$ (a) and (ECH)$_{n\beta}$-npa-(GL)$_{n\varepsilon}$|$_{(Fe3O4\rightarrow MI)}$ (b)

This paper analyzes the quantification possibilities of the morphology and topology of the nanocomposite structures based on Fe_3O_4 nanoparticles, coated with organosilane polymer of the n[SiO_{ε}-$(CH_2)_3(NH_2)$]$(NH_2)_{n\delta}$ type {where: ε = the cohydrolysed degree of the (3-aminopropyl)-triethoxysilane used in the coating process; δ = the fixing degree of the amonium and the other aminated chemical groups on the surface and in the depth of the coating layer} and functionalized with glutaraldehyde (GL) and epichlorohydrine (ECH).

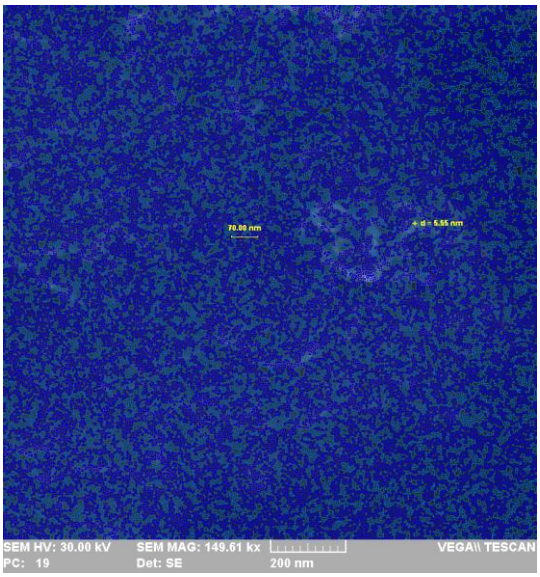

(a)

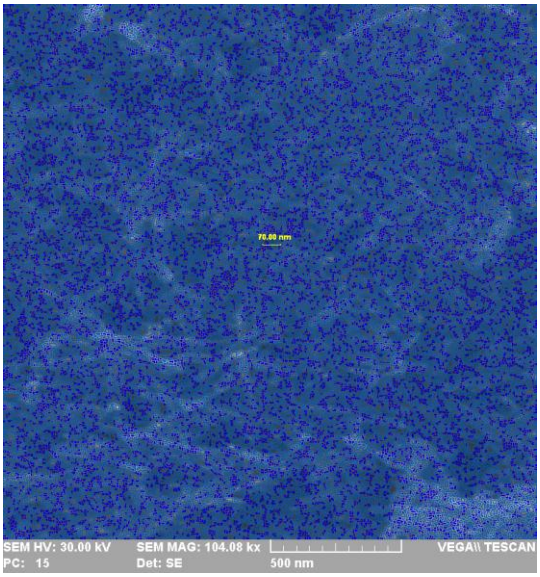

(b)

Fig.4. Acquired scanning electron image through combined spatial filters Median Filtering and Waterwash for (ECH)$_{n\beta}$-npa-(GL)$_{n\varepsilon}$|$_{(Fe3O4\rightarrow CP)}$ (a) and (ECH)$_{n\beta}$-npa-(GL)$_{n\varepsilon}$|$_{(Fe3O4\rightarrow MI)}$ (b)

2.Theoretical considerations

In most cases, the samples investigated are in physical or chemical flocculated forms. This aspect presents several inconvenients concerning the impossibility to quantify satisfactorily the morphology, topology, geometry, type and flocculation degree.

The geometric structure data were acquired using the VEGA *II* LMU scanning electron microscope, which can identify and process statistically the basic components of the investigated structure.

The neighboring structural elements (SE) are defined as points which are located at a certain distance in relation to the center of the lowest value, named threshold value [6,7].

The adaptive method of determining the neighbours needs to specify a certain mapping criterion of geometric, morphological type, etc., as well as an accepted value *m*>0 (m = tolerance), so that, in any point x one can determine the $V_m^h(x)$ neighbours, containing those y points, which observe the relation $|h(y)-h(x)| \le m$ [1]. Tolerance represents a sensitive parameter, which is dependent on the optoelectronic magnification on which the data acquisition was performed.

The optoelectronic images attached to the investigated surfaces, as well as *the maps of structural elements* (SeM) attached to the acquired optoelectronic images are shown in fig.3a, fig.3b, fig.4a, and fig.4b, respectively. Given that the nanostructures are in both agglomerated and dispersed forms and that they are physically observable, we can say that between SeM and the statistics of the specific geometric parameters (fig.5a, fig.5b) there are the following types of analytical correspondences:

- if the SeM dimensions are smaller than *the corresponding real objects* (Ro), then it can be said that a specific region of statistical distribution of the interference type, shown in fig.5a and fig.5b, corresponds to these SeM;
- if the SeM dimensions are equal to the Ro dimensions, then, one may affirm that a discreet specific region of statistic distribution corresponds to these dimensions, as shown in fig.5a and fig.5b;
- if the SeM dimensions are bigger than the Ro ones, one may assert that a specific mixed region of static distribution corresponds to these dimensions, as shown in fig.5a and fig.5b;

Fig. 5b reproduces the general model of distribution of the $N_i=f(\chi)$ graphical representation (fig.5b) {where, χ is: surface (S), length (L), width (W), perimeter (P), compactness ($P^2/4DS$) etc}. The investigation of pattern distribution can provide useful information, concerning: (a) the average dimensions of the geometric parameters attached to the nanoparticles; (b) the degree of flocculation; (c) the physical and chemical interaction processes, of the surface and interface type.

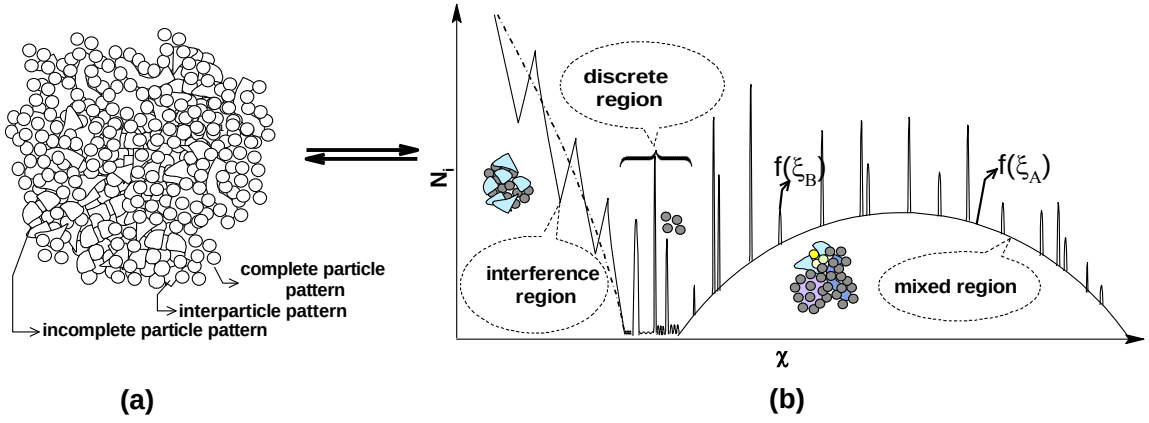

Fig. 5. The theoretical model of the elementary segmentation of the electronic scanned surface (a) and the statistically distribution regions of the elementary segmentation surface, on the acquired image (b)

Fig. 5 presents the general analytical pattern of the $N_i=f(\chi)$ function, whose analytic behaviour quantifies the morphological and topological distribution of the nanostructures and their corresponding flocculant domains.

The flocculation phenomena are generated by the occurrence of the physical and chemical surface properties. These phenomena are reflected by the formation of nanoparticle microdomains, consisting of cluster sets of nanoparticles, which are in physical and chemical association due to surface interactions.

The $N_i=f(\chi)$ function (fig.8 and fig.9) is a function which has the characteristics of a overlapped function, whose analytical profile is the result of function overlapping, of the Gaussian, exponential decay and power types. These findings were possible by analyzing the behaviour of the acquired experimental data.

The interference region (Ir) includes those patterns which are fractional compared with the real object that has generated them. According to the proposed model, Ir describes the statistical distribution of the partially hidden objects and holes in their structure. From a mathematical point of view, the statistical distribution regions of the morphological and topological structures of the Ir show object patterns that are modelled by the mathematical relations, of the type:

$$\Sigma_{i,n}\delta\chi_i\Sigma_{j,m}\delta\chi_j=f[(x_n-x_m)^2]\ f(x_n-x_m)\delta\,|\,x_n-x_m\,| \quad (5)$$

$$\delta\chi_i \leq \langle\chi_{np}\,|\,\chi_{np}\rangle \quad (6)$$

where,

χ_i = SeP with fractional value, compared to Ro

χ_{np} = the normalized value of the χ average parameter

χ_j = infinitesimal variation of the SeP fractionation surface

$\delta\,|\,x_n-x_m\,|$ = Dirac function of the delta type

From an experimental point of view, the infinitesimal variation of the geometric dimensions of SeP surfaces cannot be less than the per pixel resolution reached by the electron microscope, at the magnification achieved in the experimental data acquisition.

The direct dimensional measurements performed on the acquired optoelectronic images indicate an average value of about 5 nm of the functionalized nanoparticle diameter. One observes that the nanoparticle diameter has a narrow dispersion, as compared to $\bar{d}$ ($\bar{d}$ = the diameter mean), and that the nanoparticle topology is spherical.

As compared to the other regions of statistical distribution, *Ir* has strong discontinuity and a low degree of analytical predictability.

The discrete region (Dr) includes those isolated SeP, which are sufficiently dispersed to avoid coming into contact with one to another. In most cases, these SeP dimensions correspond to real object particles.

There are certain situations, in which the neighbouring Ir and Rd involve the indiscernible geometrical parameters f (χi), belonging to the SeP of the *Ir*, *Rd* and *Mr* regions. Most likely, this is due to the nanoparticle flocculation phenomenon, which induces the recognition of both the SeP belonging to Ro and to those derived through the neighboring SeP overlap (Fig. 5).

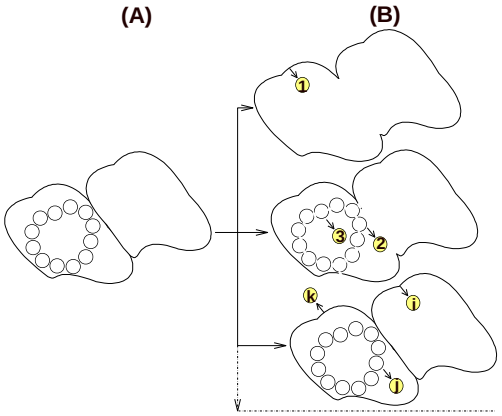

Fig. 6. Connection and association possibilities of different SeP morphological shapes during the electronic acquisition process A. Flocculated real object, resulted in the segmentation process, B. The 1, 2, ... , i, j, k, ... neighboring SeP.

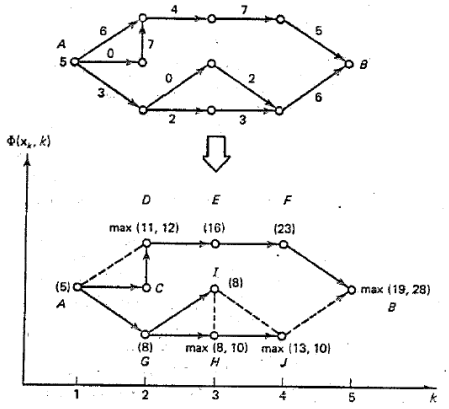

Fig. 7. Dynamic programming process for optimal boundary extraction – after A.K Jain [12]

The mixed region (Mr) includes those resulting SeP, as a result of the SeP contribution belonging to the interference and discrete regions, and whose statistical distribution is modelled by a composed function, of the type:

$$\chi_R=\chi_A+\chi_B \quad (7)$$

where,

χ_R = mixed SeP resulted in the p(x,y) point

χ_A = the SeP contribution with fractional value in the p(x,y) coordinate point

χ_B = the contribution of SeP with discreet value in the p(x,y) coordinate point

The Mr region characterises directly the degree of flocculation of the particles, the morphology and topology of the flocculated regions. This statistical distribution region results through the overlap of the Ir and Dr statistical distribution (ec.8), which are extended throughout the scanning value domain:

$$\delta\chi_R=\delta(\chi_A+\chi_C)=\chi_A+\chi_C+\varepsilon=f(\chi_A)+f(\chi_C) \quad (8)$$

where,

ε = incremental step of the χ parameter

The $f(\chi_A)$ contribution depends on the density and the composition of the morphological and topological structures that compose the flocculation microregions. In most cases which were presented in fig.8 and fig.9, the analytical form of the $f(\chi_A)$ contribution is of a semieliptic type. The large axis of the semiellipse is directly proportional to the overall size of the geometrical parameters characterizing the nanoparticle bulk domains. The small axis of the semiellipse is directly proportional to the size of the geometrical parameters specific to the nanoparticle local bulks, as well as to the number of nanoparticles contained in the structure of the local bulk domains.

The convolution function $f(\chi_A)$ overlaps the $f(\chi_B)$ function, which models the contribution of SeP having a discrete unitary value. Over the convolution function $f(\chi_A)$

overlap the function $f(\chi_B)$, the SeP contribution shaping sites with discrete unit value.

The size value and the number value of the subdomains, as main constitutive elements of the investigated flocculated domains, can be inferred from the overlap analysis of the $f(\zeta_A)$ and $f(\zeta_B)$ elementary functions.

In some cases, Ir may contain a limited number of distribution subdomains. It can be noticed that these subdomains have a discrete character and that the actual geometric dimensions are not in accordance with the geometrical measurements, which were performed directly on the optoelectronic images. For example, certain subdomains have areas of about 1-2 nm^2. This type of areas cannot be assigned to the functionalized nanoparticles, as the directly observable average sizes are distributed in the 3÷5 nm range. It follows that these areas characterize the gaps between the nanoparticles, the partially hidden nanoparticles, the microimperfections which are present on the area where the sample was submitted or the background noise.

3. Experimental data

The investigated nanostructures are Fe_3O_4 nanoparticles coated with organosilane polymers of the $n[SiO_{1.5\gamma}\text{-}(CH_2)_3(NH_2)](NH_2)_{n\delta}$ type [9,10,11]. These nanoparticles which were obtained were functionalized differently with GL and GL + ECH [8]. The functionalised nanostructures which were obtained were tested on the ricin [8], then they underwent optoelectronic investigations.

The investigated nanostructures were obtained in various functionalized forms (monovalent and polyvalent), according to Petrea et al. reports [8,9,10,11]. Also, Petrea et al. showed that these nanostructures have complex composite structure, of the $(ECH)_{n\beta}\text{-}\{Fe_3O_4\text{-}n[SiO_{1.5\gamma}\text{-}(CH_2)_3(NH_2)](NH_2)_{n\delta}\}\text{-}(GL)_{n\varepsilon}$ $\{(ECH)_{n\beta}\text{-npa-}(GL)_{n\varepsilon}\}$ type [8,9,10,11].

4. Results and discussion

To acquire SeM profiles the VEGA II LMU scanning electron microscope was used. This type of microscope can process spatially, morphologically and topologically the obtained optoelectronics images and improve their quality, by advanced statistical processing algorithms. Also, ME VEGA II LMU can perform local chemical microanalyses and maps on points and surface.

The SeM (fig. 4, fig.4b) were obtained by applying the median filtering nonlinear spatial filter to the acquired optoelectronic images. This filter is defined by the analitical relation $\nu(m,n)=\text{median}\{y(m-k,n-l)\}$ {where $(k, l) \in W$} and has the effect of replacing a given pixel with the median of the pixels contained in the dynamic scanning window [12]. The application of this type of spatial filtering is not proper to be applied to the images with high content of the rapport signal-to-noise.

The structural element links are linked contours which determine the form of structural elements and which are obtained by tracing all the connectable contours. To determine the borders of the structural elements the dynamic programming method was used. This method involves the contour map preconversion in diagrams with N levels (fig.8), and whose evaluation function [12] is:

$$S(x_1, ..., x_N, N) = \Sigma_{(k=1,N)} \left| g(x_K) \right| - \alpha \Sigma_{(K=2,N)} \left| \theta(x_k) \right| - \beta \Sigma_{(K=2,N)} \left| d(x_K, x_{K-1}) \right| \quad (9)$$

where,

x_K is the vector of the pixel contour location, at the k level of the graphic

$d(x_K,x_{K-1})$ is the Euclidian distance between two nodes

$g(x_K)$, $\theta(x_K)$ are magnitude and angle gradients, at the node level

α, β are positive parameters

The optim links which define SeM is resulted by connecting x_k nodes, so that the condition $\Phi(x_N,N)=\max_{K1, ..., xN-1}\{S(x_1, ..., x_N,N)\}$should be carried out (fig.8). The $\Phi(x_K)$ function is called the evaluation function and has the role of assessing the distance between two points, A and B, which are forced to pass through the x_K nodes [12].

The SeP perimeter is defined by $P=\int\{(x^2(t) + y^2(t)\}^{1/2}dt$, where t represents the border of the segmented objects, but not necessarily the object length.

From fig.9 it follows that the $(ECH)_{n\beta}\text{-npa-}(GL)_{n\varepsilon} \left|_{(Fe3O4 \rightarrow MI)}\right.$ perimeter has an approximate Gaussian distribution with the x_C =5.0981 pxl and w=5.0961 pxl parameters. Given that the size per pixel is of 2.66 nm (fig.10b), it results that the average length of the investigated nanostructures is of about 13.56 nm. Further, from the comparative analysis of the remaining geometrical parameters (L, W, S, $P^2/4DS$), it is found that this parameter characterizes the dimensions of the flocculation domain. From fig.3a, it follows that the directly measurable geometrical dimensions of this type of nanoparticles are of about 5 nm. The data from the parameter perimeter suggest that this type of nanoparticles prefers the formation of needle shaped flocculation domains.

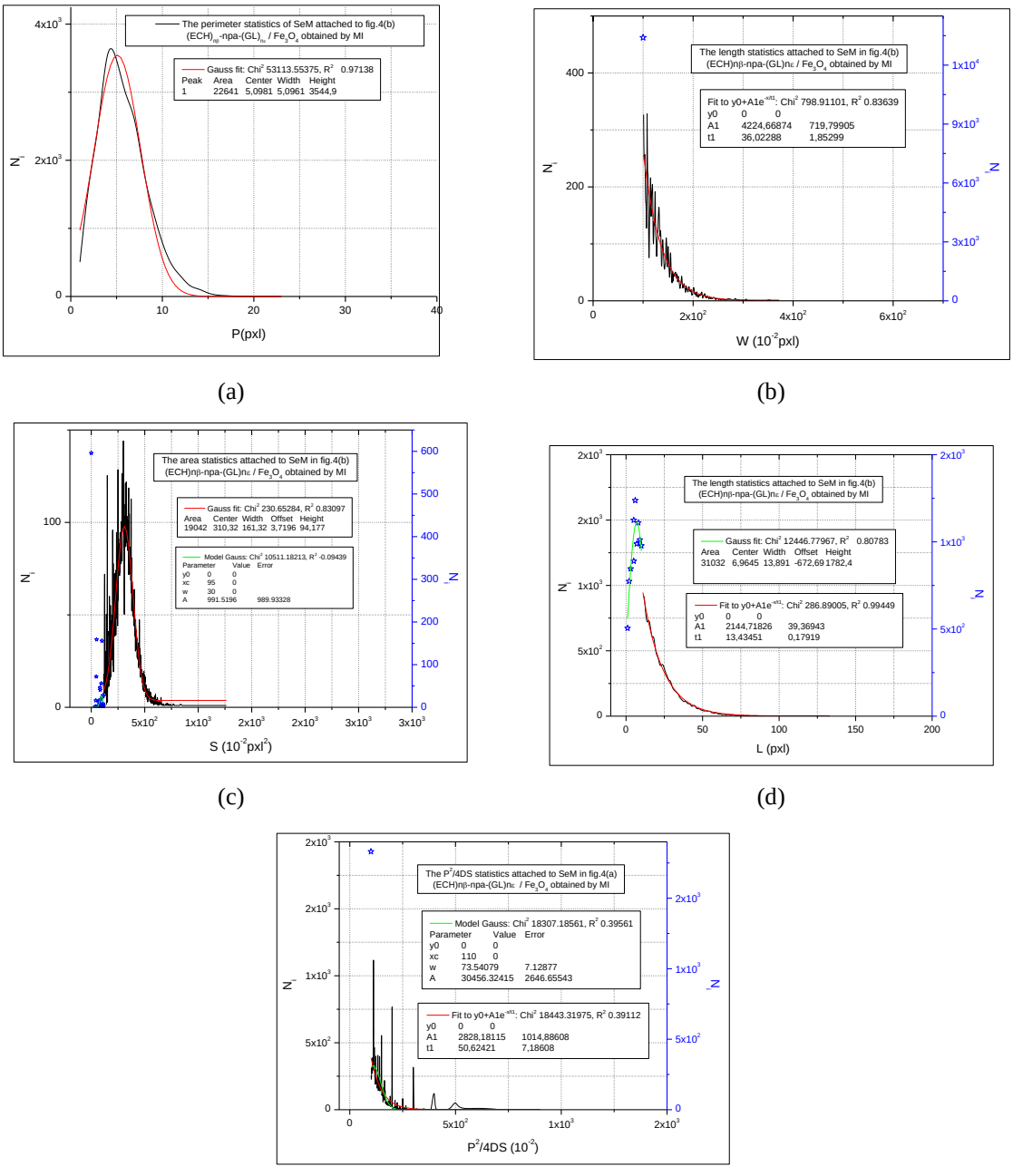

Fig. 8. The graphical representation of the f (χ) function for the case $(ECH)_{nβ}$-npa-$(GL)_{nε\ (Fe3O4→MI)}$ (a) χ=P, (b) χ=W, (c) χ=,S (d) χ=L ,(e) χ=P^2/4DS.

The $(ECH)_{nβ}$-npa-$(GL)_{nε(Fe3O4→CP)}$ perimeter has a different statistical distribution function for the analytical function, which fits the distribution points, as compared to the $(ECH)_{nβ}$-npa-$(GL)_{nε}\,|_{(Fe3O4→MI)}$ perimeter. The main trace of the statistical distribution of the perimeter for $(ECH)_{nβ}$-npa-$(GL)_{nε(Fe3O4→CP)}$ corresponds most probably to Mr and characterises the flocculation domains. Indeed, in fig.3b one can notice that the average observable dimensions of this type of nanoparticles are of about 5÷10 nm.

In the context of this analysis, the main trace can be defined as the area of distribution space, which concentrates the majority of distribution events. A key feature of this type of distribution is that the full width at half depth (FWHD) of the local distribution peaks, respectively the N_i amplitude (for any χ) have different fitting functions.

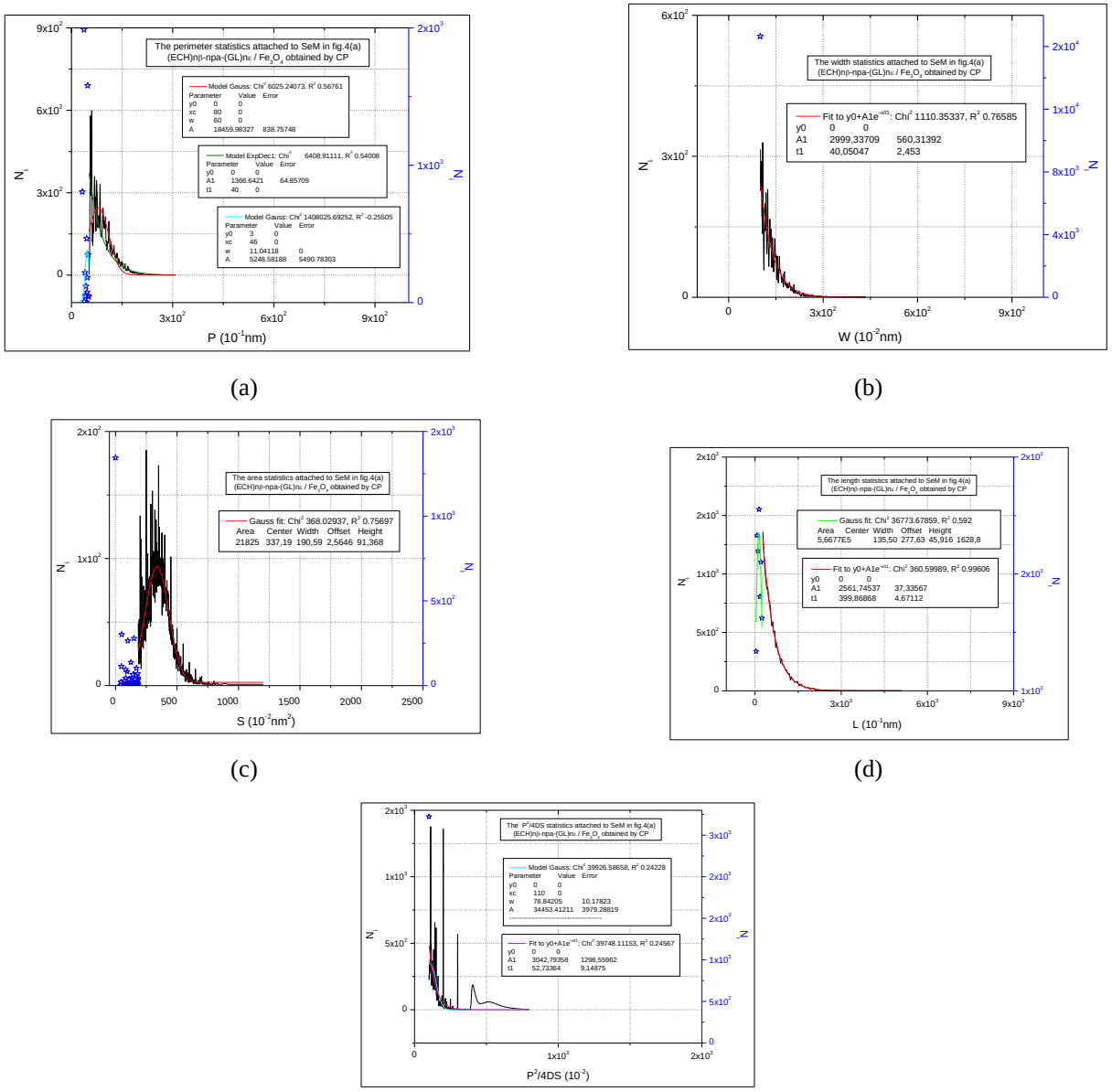

Fig.9 The graphical representation of the $N_i=f(\chi)$ function in the case of $(ECH)_{n\beta}$-npa-$(GL)_{n\varepsilon\ (Fe3O4\rightarrow CP)}$ (a) $\chi=P$, (b) $\chi=W$, (c) $\chi=S$, (d) $\chi=L$, (e) $\chi=P^2/4DS$

In turn, FWHD belonging to local statistical distributions can be fitted by distributions of the Gauss type. The function that fits the distribution of the FWHD throughout the χ definition domain, is itself a function of the Gauss type ($x_{C:P-CP}$=8 nm, w_{P-CP}=6 nm - fig.9a). The peak amplitudes of the N_i observable are fitted by an exponential decay type of function, indicating that the obtaining and flocculation processes of the $(ECH)_{n\beta}$-npa-$(GL)_{n\varepsilon}\big|_{(Fe3O4\rightarrow CP)}$, are statistical processes, whose distribution, as compared to the perimeter, is relatively narrow. From the above, it results that the mean of the nanoparticle perimeter $(ECH)_{n\beta}$-npa-$(GL)_{n\varepsilon}\big|_{(Fe3O4\rightarrow CP)}$, is of about 8 nm. This fact is in accordance with the experimental data which are directly measurable on the acquired optoelectronic images.

Close to the main trace one can notice a relatively discrete distribution region of the N_i events, which has a low density distribution of events per χ unit. By comparing the dimensions observed by directly performed measurements, one can observe a good correlation of the directly performed measurements and of the statistical distribution predictions in accordance with the proposed general correlation model. Considering these arguments, as well as the fact that the amplitude corresponding to the distribution peaks is much larger than any other $N_{i,}$ which is found throughout the χ domain of the perimeter values,

it results that this region is characteristic of the unflocculated $(ECH)_{n\beta}$-npa-$(GL)_{n\varepsilon}\big|_{(Fe3O4\rightarrow CP)}$.

In terms of the analytical point of view, the distributions of the SeP areas of the two types of functionalized nanoparticles have similar distribution patterns (fig.8c, fig.9c), but different values. In terms of the mathematical morphology, the determination of the SeP area is performed by the $S=\int_{\partial\Re}\{y(t)\,dx(t)dt/dt\}-\int_{\partial\Re}\{x(t)dy(t)dt/dt\}$ mathematical relation ($\partial\Re$ is the border of the object).

From the graphs of the two types of distribution one can deduce that the nanoparticle area $(ECH)_{n\beta}$-npa $(GL)_{n\varepsilon}\big|_{(Fe3O4\rightarrow CP)}$ has an average value of 3.37 nm^2, as compared to the average area of $(ECH)_{n\beta}$-npa-$(GL)_{n\varepsilon}\big|_{(Fe3O4\rightarrow MI)}$, which is of about 3.1*k= 8.24nm^2 (k=2.66; fig.10b).

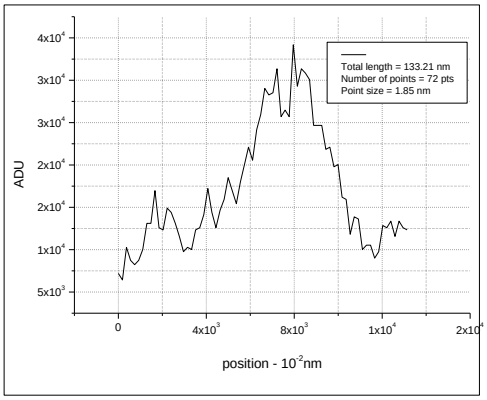

(a)

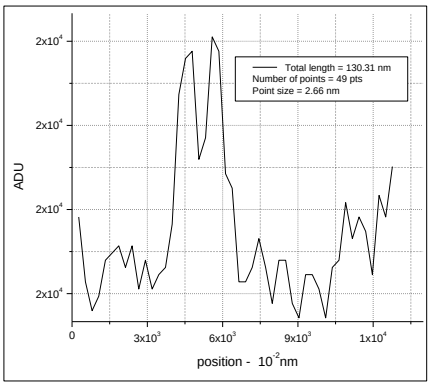

(b)

Fig.10. Linear profiles attached to optoelectronic images in fig. 3, in the case of $(ECH)_{n\beta}$-npa-$(GL)_{n\varepsilon}\big|_{(Fe3O4\rightarrow CP)}$ (a) and $(ECH)_{n\beta}$-npa-$(GL)_{n\varepsilon}\big|_{(Fe3O4\rightarrow MI)}$ (b)

The analytical profile of the Gaussian distribution of the nanoparticle surfaces is determined by the irregular morphological structure of the investigated area, which is projected in the optoelectronic image plane (fig.11b) with a signal amplitude that depends on the angle of incidence of the scanning radiation (fig.11a). The main distribution curve (fig.8c, fig.9c) is obtained by fitting the local distribution peaks, that have a Gaussian character, but with different characteristic parameters (e.g., area, center, etc.). The different mathematical nature of the local distribution peaks is due to the size of nanoparticles, to the bulk domains, as well as to the depth and masking effects, caused by the flocculation and the morphology of the nanoparticle bulk.

From the graphs of statistical distributions (fig.8c, fig.9c) one can deduce the size peak value of the bulk domains. Thus, it follows that the specific flocculation domains, which are specific to the $((ECH)_{n\beta}$-npa-$(GL)_{n\varepsilon}\big|_{(Fe3O4\rightarrow MI),}$ have an average area of (12.63-0.91)*k=31.17 nm^2, and the flocculation domains specific to $(ECH)_{n\beta}$-npa-$(GL)_{n\varepsilon}\big|_{(Fe3O4\rightarrow CP)}$ have an average area of (11.83-1.85)=9.98 nm^2.

Indeed, by comparing the acquired optoelectronic images in figures 3a and 3b, with the calculated values resulted after having used the elementary segmentation method, it follows that the area is the geometrical parameter that characterizes both the nanoparticle size and the size of the flocculation domains. In addition, the resulted bulk domains, both in the case of the $((ECH)_{n\beta}$-npa-$(GL)_{n\varepsilon}\big|_{(Fe3O4\rightarrow CP)}$, as well as in the case of $(ECH)_{n\beta}$-npa-$(GL)_{n\varepsilon}\big|_{(Fe3O4\rightarrow MI}$ contain approximately three nanoparticles.

This fact leads to the idea that the main flocculation mecanism in the case of these nanoparticle types is the micromagnetic type, by forming local, stable and closed, magnetic domains.

In terms of mathematical morphology, the quantification of the length and the width of objects implies the determination of the smallest rectangle enclosing the object identified by SeP technique , as well as its orientation ($\alpha = x*\cos\theta + y*\sin\theta$, $\beta = - x*\sin\theta + y*\cos\theta$, where, α_{min}, α_{max}, β_{min}, β_{max} are connecting conditions). Thus, $W = \beta_{min} - \beta_{max}$ determines the SeP width, and $L = \alpha_{min} - \alpha_{max}$ determines their length [12].

With respect to the $(ECH)_{n\beta}$-npa-$(GL)_{n\varepsilon}\big|_{(Fe3O4\rightarrow MI)}$, the SeP width has two distribution regions, which differ in terms of analytic behavior (fig.8b, fig.9b). The first region (blue stars) consists of a singular point for which the amount $N_i \triangleq N_s$ is much greater than that of any N_i which is distributed on the W definition domain, so that $N_i=f(W)$. The second region (black continuous line) consists of the $N_i \rightarrow W_i$ points, whose value is much smaller than the amplitude of the $N_i \triangleq N_s$ point. The $N_i \rightarrow W_i \backslash N_s$ point distribution throughout the definition domain of the W parameter is described by a fitting law of the exponential decay type. The δW domain ($W_{i\text{-}MI}$=1.85 nm; $W_{f\text{-}MI}$~6.8 nm), for which N_i tends to zero, is small in terms of value and approximately equal to the average diameter size of the nanoparticles derived by direct optoelectronic measurements. Taking into account the fact that the elecronic scan was performed only on the sample surface (fig.3, fig.3b) the singularity point most likely belongs to the Ir region and quantifies, in general, the space connected contours between SeP. Since the $N_i=f(W)$ function is not continuous in the singularity point (W_s=1.85 nm, N_s=13.406) and assuming that the W=1.85 nm point describes the distribution of the contours, which

are specific to the interference region, it is likely that the singularity point should describe the minimum neighbouring distance between the neighbouring functionalized nanoparticles, as a result of the micromagnetical, microelectrical and morphochemical interactional types.

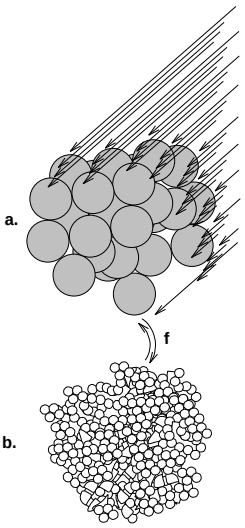

Fig. 11. The influence of the depth, masking and shading phenomena on the image elementar segmentation process real clustered objects in scanning process, b. SeP sites identified on the acquired image via f object-to-image signal transfer function

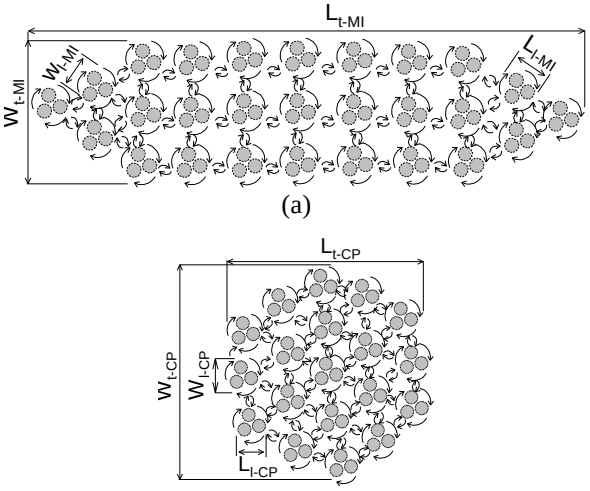

Fig. 12. The real nanocomposite morphology of $(ECH)_{n\beta}$-npa-$(GL)_{n\varepsilon(Fe3O4\rightarrow MI)}$ (a) and $(ECH)_{n\beta}$-npa-$(GL)_{n\varepsilon(Fe3O4\rightarrow CP)}$ (b), resulted as a consequence of the analysis of the experimental data WT, WL, Lt., LL = local geometric dimensions, namely the full bulk domains.

The same analytical behavior is also observed in the case of the statistical distribution of the functionalized nanoparticle width obtained by MI. The width of statistical distribution $(ECH)_{n\beta}$-npa-$(GL)_{n\varepsilon}\,|_{(Fe3O4\rightarrow CP)}$ has its own different parameters (δW: $W_{i\text{-}CP}$=1 nm, $W_{f\text{-}CP}$~4.3 nm).

The difference between the $W_{i\text{-}(Fe3O4\rightarrow CP)}$ and $W_{f\text{-}(Fe3O4\rightarrow MI)}$ points, which delimits the W_s point from the rest of the distribution domain is due, up to a constant, to different incremental steps, used in the segmentation and acquisition process of the two investigated cases of SeM (pxl, nm).

Both in the case of the $npa_{(Fe3O4\rightarrow CP)}$, and the $npa_{(Fe3O4\rightarrow MI)}$, the length statistics can be divided into two regions, which, analysed according to the correspondence model, prosed in fig.5, can be attributed to the Dr (blue stars) and Mr (black points joined by continuous lines black). As for Dr which is proper to statistics $((ECH)_{n\beta}$-npa-$(GL)_{n\varepsilon}\,|_{(Fe3O4\rightarrow CP)}$, the function fitting the SeP length distribution is a Gaussian one, having $x_{C\text{-}DR}$=13.55 nm, w_{DR}=27.76 nm parameters (fig.9d).

The function that fits the length distribution of the nanoparticles on the Mr region is of the exponential decay type and has its eigenvalue parameters $\Delta w_{Dr\text{-}CP}$=482.6 nm ($L_{i\text{-}DR}$=27.4 nm; $L_{f\text{-}DR}$=510 nm).

Similarly, with respect to the statistics of the SeP length specific to the $(ECH)_{n\beta}$-npa-$(GL)_{n\varepsilon}\,|_{(Fe3O4\rightarrow MI)}$, we have the following characteristic parameters: $x_{C\text{-}DR}$=6.96*k=20.6 nm, w_{DR}=13.89*k=36.94 nm, $\Delta w_{Dr\text{-}CP}$=(132.87-10.93)*2.66=324.33 nm.

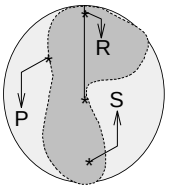

Fig.13. The correspondence between the geometrical dimensions of the real objects and the value of the $P^2/4DS$ parameter

The compactness (roundness) parameter of the SEP is an overlapped function, which is used to connect analytically the following parameters: perimeter, area and diameter (fig.13), which are specific to the object nanostructures. Considering the fact that there is a close relationship between the contour of a given area and the area which is delimitated by the corresponding contour, it follows that compactness is a direct measure of the degree of coherence of the nanostructure morphology. This coherence translates through a directly measurable link, of the $D=g(P^2,S)$ type between the diameter of the circle which inscribes the respective nanostructure, and its perimeter and area. Being a very sensitive function to the morphological variations, the compactness parameter quantifies directly the nanostructure form, the number and size of the flocculated domains. As compactness is an overlapped function, it borrows a series of characteristic properties, which are specific to the component functions. As in the case of the other geometric parameters, which were previously studied, one notices that the distribution of $(ECH)_{n\beta}$-npa-$(GL)_{n\varepsilon}\,|_{(Fe3O4\rightarrow CP)}$ and $(ECH)_{n\beta}$-npa-$(GL)_{n\varepsilon}\,|_{(Fe3O4\rightarrow MI)}$ is composed of regions having different analytical properties, corresponding to the Dr, respectively Mr regions. The distribution corresponding to the Mr

region can be fitted by a distribution function of the exponential decay type (relative to the amplitude of the local distribution peaks), or of a Gaussian distribution function type (relative to the FWHD distribution attached to the local distribution peaks).

The singularity point, corresponding to Dr, is one in value, which corresponds to the nanoparticles with a roughly spherical morphology.

It was observed that, in the case of $(ECH)_{n\beta}$-npa-$(GL)_{n\varepsilon}\big|_{(Fe3O4\rightarrow CP)}$, the Mr region has seven local peaks, which are clearly defined, and which most likely describe the analytical structure of the local flocculation domains (fig.9e). the compactness of this type of nanostructure has values in the 1.1÷7.88 range. The local flocculation domains are connected by bridges of unflocculated nanoparticles, relatively uniformly distributed.

With respect to the $(ECH)_{n\beta}$-npa-$(GL)_{n\varepsilon}\big|_{(Fe3O4\rightarrow MI)}$, the compactness distribution contains nine local flocculation domains, and has values in the 1.1÷9 (fig.8e) range.

Figs. 12.a and 12.b indicate the morphology and the flocculation domains adopted by the $(ECH)_{n\beta}$-npa-$(GL)_{n\varepsilon}\big|_{(Fe3O4\rightarrow CP)}$ and $(ECH)_{n\beta}$-npa-$(GL)_{n\varepsilon}\big|_{(Fe3O4\rightarrow MI)}$ nanostructures. Given the regularity of the flocculation domains, it can be assumed that the main flocculation mechanism is of the micromagnetic type, which induces the formatin of closed magnetic microdomains. As a result of the analysis of the acquired numerical data, relative to the size of the nanoparticles and the local dimensions of the flocculation domains, it follows that the material suspension is chemically stable and it does not present significant secondary chemical crosslinked processes of the self type.

5. Conclusions

This paper proposes a quantification analytical method for the investigatin of the morphological and morphochemical charateristics of the nanostructured materials. To extract predictive information on the processing of the statistical data, a phenomenological correlation model was proposed in order to explain the distribution patterns, according to the morphological and morphochemical properties of the generating structure.

The data which were obtained and interpreted according to the analytical model of correlation of the statistics of the perimeter, length, width, area and compactness morphological parameters are in accordance with the optoelectronic measurements, which were performed directly on the acquired images, as well as with the functionalization mechanisms, which are induced in the surface functionalization processes.

The structural element map method proved to be a very sensitive tool for investigation of the surface chemical and physical effects, of the following types: crosslinking processes, interface energy, surface energy, microelectrical, micromagnetical, flocculation density, etc.

It was also established a univoque correspondence between the morphological parameters and the corresponding physical and chemical processes which are responsible for the modelling of these parameters.

Acknowledgments

The authors are grateful for the financial support granted by the Research and Education Ministry of Romania (projects no. 31-001/2007, 81-002/2007, 32-165/2008 – within the National Plan for Research and Innovation) and for the logistic support granted by the Scientifical Research Center for CBRN Defense and Ecology.

References

[1] P. Maragos, C. Vachier, ICIP, 2241-2244 (2009).
[2] E. R. Dougherty, R. A Lotufo, Hands-on Morphological Image Processing, SPIE PRESS (2003).
[3] I. N. Bouaynaya, C. Chefchaouni, D. Schonfeld, IEEE Tr-PAMI, **30**(5), 823 (2008).
[4] B. J. Pastore, B. A. Bouchet, E. Moler, V. Ballarin, JCS&T, **6**(2), 80 (2006).
[5] J. Serra, Image Analysis and Mathematical Morphology: Theoretical Advances, **2**, Acad. Press, NY, 1988.
[6] J. C. Russ, The Image Processing Handbook, 3rd ed., CRC Press (1998).
[7] E. B. Corrochano, Handbook of Geometric Computing - Applications in Pattern Recognition, Computer Vision, Neuralcomputing, and Robotics, Springer (2005).
[8] N. Petrea, P. Z. Iordache, V. Şomoghi, I. Savu, M. Mureşan, R. Petre, L. Rece, R. Lungu, A. Pretorian, G. Mitru, B. Dionezie, B. Savu, L. Mutihac, L. Kim, V. Ordeanu, DJNB **4**(4), 699 (2009).
[9] P. Z. Iordache, V. Şomoghi, N. Petrea, R. Petre, B. Dionezie, V. Ordeanu, A. Hotăranu, L. Mutihac, J. Optoelectron. Adv. Mater. **11**(5), 736 (2009).
[10] P. Z. Iordache, V. Şomoghi, I. Savu, N. Petrea, G. Mitru, R. Petre, B. Dionezie, V. Ordeanu, L. Kim, L. Mutihac, Optoelectron. Adv. Mater. - Rapid Comm., **2**(8), 491 (2008).
[11] P. Z Iordache, V. Şomoghi, I. Savu, N. Petrea, G. Mitru, R. Petre, B. Dionezie, V. Ordeanu, A. Hotaranu, L. Mutihac, Rev. Chim., Plastics Materials, **46**(2), 162 (2009).
[12] A. K. Jain, Fundamentals of Digital Image Processing, Prentice-Hall (1989).
[13] T. S. Huang, A. B. S. Hussain, IEEE Trans. Commun., COM-23, **12**, 1452 (1975).
[14] J. C. Pinoli, J. Debayle, EURASIP J ADV SIG PR, ID 36105 (2007).

*Corresponding author: iordachezamora1978@gmail.com